20th Australasian Fluid Mechanics Conference
Perth, Australia
5-8 December 2016

An Investigation of the Application of Discontinuous Galerkin Method for Conjugate Heat Transfer of Thermoelectric Cooler

Z.Cai[1] and B.Thornber[2]
[1&2] The University of Sydney, School of Aerospace,
Mechanical and Mechatronic Engineering, NSW, 2000, Australia

Abstract

The thermoelectric cooling module has been widely used in the optical communication industry to maintain a stabilized temperature gradient in core optical components. The design of modern optoelectronic devices relies on the accurate numerical prediction of thermal loading on the hot-end components. The purpose of this paper is to present an approach applying the Discontinuous Galerkin (DG) method to conjugate heat transfer (CHT) simulations. The incompressible Navier-Stokes (INS) equations under the Boussinesq assumption and solid heat equation are simultaneously discretised using an explicit DG formulation. A Dirichlet-Neumann partitioning strategy has been used to couple the heat fluxes between the solid and fluid domain, as well as heat transfer among multi solid domains. The stability of the methodology has been validated by several benchmark cases. The numerical results have shown good convergence in P and H refinement in both fluid dynamics and CHT problems.

Introduction

A thermoelectric cooler (TEC), sometimes called thermoelectric module or peltier cooler, is a semiconductor based electronic component that functions as a small heat pump. By applying a low voltage DC power source to a TEC module, heat will be moved through the module from one side to the other. This phenomenon can be reversed by a change in the polarity of the applied DC voltage. The thermoelectric module is widely used for both heating and cooling thereby making it highly suitable for precise temperature control applications, such as solar-based thermoelectric technologies, CPU cooling, power generation system, optical and laser system. There are mainly two approaches to model the TEC: detailed modelling approach and compact modelling approach. The first approach is to numerically model every thermo-element in a TEC. Chen [1] presented a three-dimension numerical study for TEC consists of 8, 20 and 40 pairs of thermo-couples via mainly concerning on the influence of scaling effect and Thomson effect on the cooling performance. This detailed modelling method was extended to transient analysis [2] and the multi-stage TEC [3]. Instead of modelling each thermo-element individually, another major approach is to model the TEC module as a single bulk block, which is referred as the compact thermal modelling method. This method can handle the multi-scale issue using fine mesh and coarse mesh at different region respectively. The implement of this method can be found in [4].

Discontinuous Galerkin (DG) methods belong to the class of finite elements. The finite element function space corresponding to DG methods consists of piecewise polynomials (or other simple functions) which are allowed to be completely discontinuous across element interfaces. The DG method has in particular received considerable interest for the area of aero-acoustics, electro-magnetism, air dynamics, modelling of shallow water and weather forecasting, among many others. The first DG method was introduced in 1973 by Reed & Hill [5] to solve the steady state neutron transport equation. This method was later generalised by Cockburn [6] and Bassi [7] to inviscid laminar and turbulent flows. Compared to the traditional finite element method, the mass matrix in DG method is local rather than global and thus can be inverted by very little cost. The DG method can also achieve higher order accuracy in the problem with complex geometry or poor quality meshes.

The introduction of DG methods to the whole domain of conjugate heat transfer (CHT) problems can be a benefit for improving the accuracy in the region around the interface and localising the data exchange process, and further enhancing the convergence and stability of the entire computation in some degree. Zengrong [8] implemented a centroid-expanded Taylor basis DG method to the compressible fluid dynamic equations and solid heat conduction equations to solve turbo-machinery problems. Huafei [9] proposed a simplex cut-cell technique, where the interface definition is completely separate from the mesh generation process to solve CHT problem. This technique shows high-order convergence for CHT problems with non-smooth interface shapes.

The main contribution of this paper is to present a framework for the simulation of CHT problems by applying DG methods on unstructured grids. Based on an existing DG solver for the INS equation [10], the Boussinesq assumption term and solid heat equation are included by using an explicit DG formulation. A Dirichlet-Neumann partitioning strategy has been implemented to achieve the data exchange process via the numerical flux of interface quadrature points in both fluid-solid and solid-solid interface. All the modelling equations are solved using the DG methods as the basis equations. Two benchmark cases are presented to validate the Boussinesq assumption term and the solid heat equation. All the numerical results have shown good convergence in both P and H refinement.

Discontinuous Galerkin Method for Fluid and Solid Domain

Governing equations for the fluid domain

The Boussinesq approximation is invoked to couple the temperature and flow field. The governing equation for the steady-state two-dimension flow using the INS equations and energy equation can be written with following dimensionless variables:

$$X=\frac{x}{L},Y=\frac{y}{L},U=\left[\frac{uL}{\alpha_f};\frac{vL}{\alpha_f}\right],P=\frac{pL^2}{\rho_f\alpha_f^2},\alpha_s=\frac{k_s}{(\rho C_p)_s},\alpha_f=\frac{k_f}{(\rho C_p)_f},$$

$$Pr=\frac{\nu}{\alpha_f},\ Ra=\frac{g\beta(T_q-T_s)L^3Pr}{\nu^2} \quad (1)$$

$$\nabla\cdot U=0 \quad (2)$$

$$(U\cdot\nabla)U=-\nabla P+Pr\nabla^2U+Ra\,Pr\frac{\partial T_f}{\partial Y} \quad (3)$$

$$(U\cdot\nabla)T_f=\alpha_f\nabla^2T_f \quad (4)$$

Here subscript f and s is for the fluid and solid phases respectively. X and Y are dimensionless coordinates varying along horizontal and vertical directions respectively; U are dimensionless velocity components in the X and Y directions; u and v are velocity components in X and Y direction respectively; T_f is the fluid temperature. ν is the kinematic viscosity; ρ_f and ρ_s are the density of solid and fluid phases respectively; k_s and k_f are thermal conductivity of solid and fluid medium respectively; $(Cp)_s$ and $(Cp)_f$ are heat capacity of solid and fluid medium respectively; α_s and α_f are thermal diffusivity in solid and fluid phases respectively; T_q and T_s are the quiescent temperature and surface temperature respectively; P is the dimensionless pressure and p is the pressure; L is the characteristic length; Ra and Pr are Rayleigh and Prandtl number respectively.

The solution methodology of the INS equation (Eqs.2-3) is strictly following Hesthaven's INS-DG solver [10] where the full INS equation is break into three stages. The first conservation law components is solved using an Adams-Bashforth second-order scheme, the nonlinear term $\mathcal{N}$ and $\mathcal{F}$ are defined in Eqn.5：

$$\mathcal{N}=\begin{bmatrix} u^2 & uv \\ uv & v^2 \end{bmatrix};\mathcal{N}=\nabla\cdot\mathcal{F} \tag{5}$$

the second stage involves the projection of the updated velocity components onto the pressure term and at the final stage, the viscous term is treated implicitly.

The nonlinear term $\mathcal{N}$ in the advection stage is discretised using the Lax-Friedrichs flux based on DG discretization in the domain D^k with boundary ∂D^k：

$$(\phi_h,\mathcal{N})_{D^k}=\left(\phi_h,\nabla\cdot\mathcal{I}_N\mathcal{F}(u_h)\right)_{D^k}-\frac{1}{2}(\phi_h,[\![\mathcal{I}_N\mathcal{F}(u_h)]\!])_{\partial D^k}+\frac{\lambda}{2}(\phi_h,\hat{n}\cdot[\![u_h]\!])_{\partial D^k};\forall\phi_h\in V_h,V_h=\oplus_{k=1}^{K}P_N(D^k) \tag{6}$$

where $\mathcal{I}_N f$ refer to the N-th-order interpolation of f and V_h is a piecewise polynomial basis. The Boussinesq approximation is also interpolated at this stage:

In order to solve the pressure and viscous stage, an interior penalty Discontinuous Galerkin method based Poisson solver for curved elements [11] is implemented to solve the Poisson equation $-\nabla^2 u=f$. The detailed DG discretization is implement in Eqn.7:

$$\begin{aligned}&(\nabla\phi_h,\nabla p_h)_{D^k}-\frac{1}{2}(\hat{n}\cdot\nabla\phi_h,\hat{n}\cdot[\![p_h]\!])_{\partial D^k\setminus\partial\Omega}\\&-\left(\phi_h,\hat{n}\cdot\{\{\nabla p_h\}\}\right)_{\partial D^k\setminus\partial\Omega}+\left(\tau^k\phi_h,\hat{n}\cdot[\![p_h]\!]\right)_{\partial D^k\setminus\partial\Omega}\\&-(\hat{n}\cdot\nabla\phi_h,p_h^-)_{\partial D^k\cap\partial\Omega^o}+\left(\tau^k\phi_h,p_h^-\right)_{\partial D^k\cap\partial\Omega^o}\\&-(\phi_h,2\hat{n}\cdot\nabla p_h^-)_{\partial D^k\cap\partial\Omega^{IWC}}=\left(\phi_h,-\frac{\gamma_0}{\Delta t}\nabla\cdot\tilde{u}\right)_{D^k}-(\hat{n}\cdot\\&\nabla\phi_h,p^o)_{\partial D^k\cap\partial\Omega^o}+\left(\phi_h,\beta_0\frac{\partial p_h^n}{\partial\hat{n}}+\beta_1\frac{\partial p_h^{n-1}}{\partial\hat{n}}\right)_{\partial D^k\cap\partial\Omega^{IW}}\\&+\left(\tau^k\phi_h,p^o\right)_{\partial D^k\cap\partial\Omega^o}\end{aligned} \tag{7}$$

where $\partial\Omega^D$ and $\partial\Omega^N$ are the boundary with Dirichlet and Neumann boundary condition respectively.

The convection, pressure and viscous components are integrated in Eqn.8:

$$\frac{\gamma_0 u^{n+1}-\alpha_0 u^n-\alpha_1 u^{n-1}}{\Delta t}=-\nabla\bar{p}^{n+1}-\beta_0 N(u^n)-\beta_1\mathcal{N}\left(u^{n-1}\right)+\nu\nabla^2 u^{n+1} \tag{8}$$

where $\gamma_0=0$, $\alpha_0=1$, $\alpha_1=0$, $\beta_0=1$, $\beta_1=0$ at the first time step to start the scheme. The subsequent time steps are done with $\gamma_0=1.5$, $\alpha_0=2$, $\alpha_1=-0.5$, $\beta_0=2$, $\beta_1=-1$.

The fluid energy equation (Eqn.4) is solved following the similar manner as the INS equation as shown in Eqn.9:

$$\frac{\gamma_0 T_f^{n+1}-\alpha_0 T_f^n-\alpha_1 T_f^{n-1}}{\Delta t}=-\beta_0 H(T_f^n)-\beta_1\mathcal{H}\left(T_f^{n-1}\right)+\alpha_f\nabla^2 T_f^{n+1} \tag{9}$$

where the nonlinear Term $\mathcal{H}$ is defined as $\mathcal{H}=[U\cdot T_f]$.

Governing equations for the solid domain

The governing equation for the steady-state two-dimension heat equation in solid domain is integrated in Eqn.10:

$$\frac{q}{(\rho C_p)_s}=\alpha_s\nabla^2 T_s \tag{10}$$

where q is the heat generated per unit volume.

Similar to the viscous part of the INS equation, the solid heat equation is discretized by Eqn.7 and solved by Eqn.11:

$$\frac{\gamma_0 T_s^{n+1}-\alpha_0 T_s^n-\alpha_1 T_s^{n-1}}{\Delta t}=\alpha_s\nabla^2 T_s^{n+1} \tag{11}$$

Fluid-Solid and Solid-Solid Interface

A loosely-coupled Dirichlet–Neumann partitioning approach [12] is used to ensure the continuity in physics of the temperature and normal heat flux on the fluid-solid and solid-solid interface. At each time step, the value of temperature computed from the side of the high conductivity domain is specified as a Dirichlet boundary condition to the side of low conductivity domain meanwhile that of normal heat flux computed from the side of low conductivity domain is specified as the Neumann Boundary condition on the side of high conductivity domain and the updated data will be treated as new boundary conditions of respective domains in the next time step. Due to the nature of the DG method, all the above data exchange can be directly achieved via the numerical flux calculations at quadrature points of the interface.

TEC Compact Thermal Model

A typical TEC module is connected by many semiconductor legs between the cold and hot ceramic substrates. The full TEC module is simplified into a compact thermal model [4] within three sections as shown in Figure 1. Two ceramic substrates are modelled as top and bottom blocks while all thermo elements and interconnect metal bridges are represented as the middle macro block.

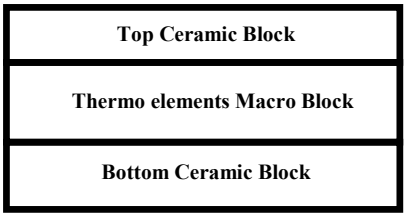

Figure 1. TEC Compact Model

The effective average TEC properties α, ρ, k can be derived from manufacture $\Delta T_{max}, I_{max}, Q_{max}$ by Eqs.12-14:

$$\alpha=\frac{Q_{max}(T_h-\Delta T_{max})}{NT_h^2 I_{max}} \tag{12}$$

$$\rho=\frac{Af(T_h-\Delta T_{max})^2 Q_{max}}{2lN^2 T_h^2 I_{max}^2} \tag{13}$$

$$k=\frac{l(T_h-\Delta T_{max})^2 Q_{max}}{AT_h^2\Delta T_{max}} \tag{14}$$

Where α, ρ, k are effective Seebeck coefficient, effective electrical resistivity and effective thermal conductivity respectively, $\Delta T_{max}, I_{max}, Q_{max}$ are the maximum temperature difference, maximum module current and maximum rate of heat

transfer respectively; T_h and T_c are TEC hot and cold side temperature respectively; N, A,I ,l, f is the number of thermal couple in the TEC, uniform cross-sectional area of the entire TEC, TEC operating current, thermoelectric element height and the packing fraction of total TEC area covered by TEC elements respectively. Compared to the detailed modelling method, the compact modelling method is more convenient for engineers to compare the performance between different brands of TEC because TEC performance curve will be generally posted while only very limited TEC manufacturer will provide their temperature dependent pellet material properties which are essential for the detailed modelling method.

The heat generation rate due to Peltier effect can be obtained by Eqn.15:

$$Q_h = 2N\alpha IT_h, Q_c = -2N\alpha IT_c \quad (15)$$

The heating and cooling heat loads (Q_h and Q_c) are applied as surface heat loads placed at two interfaces between bottom/top substrates and the middle TE block.

The joule heating load Q_j is expressed in Eqn16:

$$Q_j = I^2R,\ R = \frac{N^2}{Af} 4\rho \quad (16)$$

where R is the module resistance. This heat load is implemented as a volume heat load on all the cells of the middle block.

Benchmarks and Validations

Buoyancy Driven Cavity

The first validation case is to simulate a steady-state Boussinesq flow within a closed square cavity [13]. The INS equations and the energy equation can be validated through this benchmark case. The fluid of Prandtl number 0.71 is within a square cavity ($0 \le x \le 1$, $0 \le y \le 1$) with the following boundary conditions; both components of the velocity are set to be zero on all the boundaries, the boundary at y=0 and 1 are insulated while the temperature at x=0 and x=1 are set to be $T_1=1$ and $T_2=0$ respectively, the Rayleigh number Ra=1000. The average Nusslet number on the hot wall under different mesh size (H) and polynomial order (P) are shown in Figure 2. All simulations convergence and are in well agreement with the earlier work done by Davis in 1983 [13]. The temperature and velocity profile in fluid domain are shown in Figure 4 and 5 respectively.

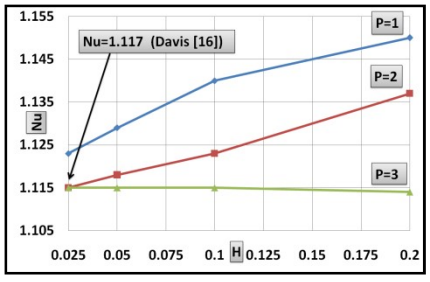

Figure 3. Comparison of average Nusselt number on hot wall as a function of mesh size and polynomial order(Ra=1000)

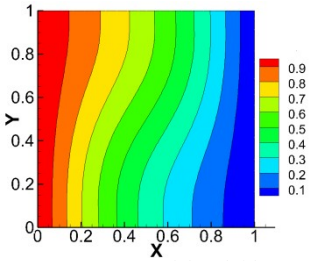

Figure 4. Temperature Contour of the Fluid Domain, Ra=1000

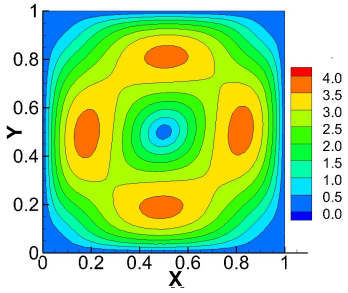

Figure 5. Velocity Contour of the Fluid Domain, Ra=1000

Conjugate Natural Convection in a Closed Cavity

he fluid configuration of the second validation case is similar to the buoyancy driven cavity while a finite thickness solid wall is attached on the hot side of the cavity. This test case can be used to validate the solid heat equation and the Dirichlet–Neumann partitioning approach. The Boussinesq fluid of Prandtl number 0.7 is within a square cavity($0 \le x \le 1$, $0 \le y \le 1$) with the following boundary conditions; both components of the velocity are set to be zero on all the boundaries, the boundary at y=0 and 1 are insulated while the temperature at x=0 are set to $T_1=0$, the Rayleigh number Ra=1000, thermal diffusivity α_f is set to 1. The solid domain($1 \le x \le 1.2$, $0 \le y \le 1$) is configured with following boundary conditions; the boundary at y=0 and 1 are insulated while the temperature at x=1.2 are set to $T_2=1$. Under the case with solid thermal diffusivity α_s =1, the average Nusslet number on the cold wall under different H and P are shown in Figure 6. All simulation results show a good convergence trend and converged results match well with the reference [14]. The temperature and velocity contour for fluid and solid domains (Ra=1e5, α_s=10) are shown in Figure 7 and 8 respectively.

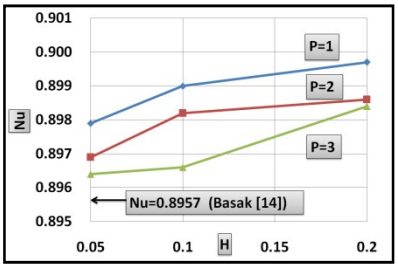

Figure 6. Comparison of average Nusselt number on Cold wall as a function of mesh size and polynomial order(Ra=1000)

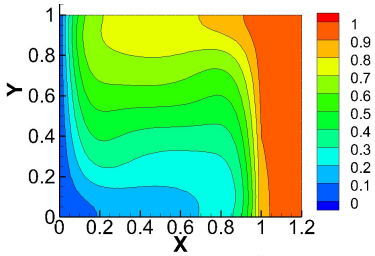

Figure 7. Temperature Contours of the Full Domain, Ra=1e5, α_s=10

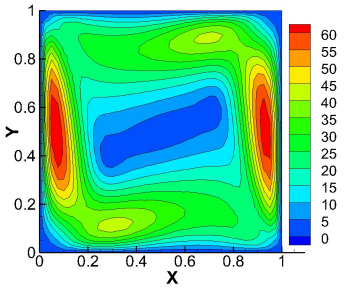

Figure 8. Velocity Contours of the Full Domain, Ra=1e5, α_s=10

TEC Compact Thermal Model

The third validation case is to simulate the performance of the TEC by a 'black box' like model [4] based on the manufacture's datasheet. In order to match up with the standard TEC performance test setup, only the solid thermal solver (Eqn.4) is enabled and the effect of fluid convection is neglected. The configuration of the TEC compact thermal model are shown in Figure 8 with following boundary conditions; the boundary at x=0 and t_1 are insulated while the temperature at y=0 are set to T_1=300K ,this is also defined as TEC hot side temperature ; Q_1 is the external heat load applied on the TEC module, the heat generation rates (Q_c and Q_h) due to Peltier effect can be obtained by Eqn.15 and are applied as surface heat loads between the interaction of the Top/Bottom block and the middle block; the joule heating heat load Q_j can be obtained from Eqt.16 and is applied as a volume heat load in all cells of the middle block. The middle block material properties can be derived from Eqs.12-14 while the conductivity of Top/Bottom ceramic is set to be 29W/mK. The MC10-049-10 from RMT Ltd is chosen as a reference TEC to verify this compact modelling method. This 15.0x15.0x2.0mm TEC has 49 thermal couples with following properties: While T_h=300K, Q_{max}=16.61W, Imax=4.46A, ΔT_{max} = 71K; the pellet dimension equals to 1.0x1.0x1.0mm. Figure 9 compares performance curves between supply datasheet and current simulation results. The different between two curves are below 1.5K under all cases. The temperature contour of the MC10-049-10 under Q_1=6W and 1.2A operating current is shown in Figure 10.

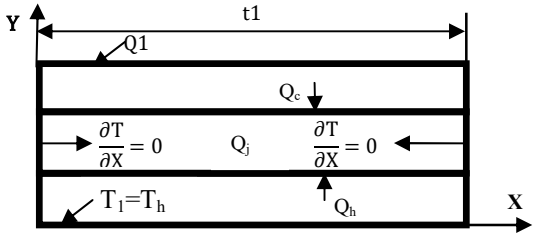

Figure 8. TEC Compact Thermal Model Configuration

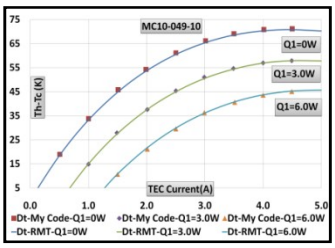

Figure 9. Temperature difference comparison of MC10-049-10 between compact simulation and supply data

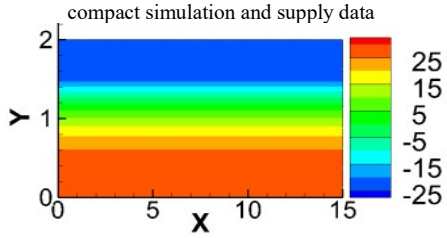

Figure 10. Temperature contour of MC10-049-10 (Q1=6W,I=1.2A)

CONCLUSIONS

In this paper, we have presented a framework for the simulation of the CHT problems on unstructured meshes by using the DG method. A loosely-coupled Dirichlet–Neumann partitioning approach is used for data exchange through the fluid-solid and solid-solid interfaces based on the numerical flux of quadrature points. The INS equations under the Boussinesq assumption, fluid energy equation and solid heat equation are solved by using the DG algorithm. A series of test cases are carried out to validate the stability the DG methodology. Good convergence is observed in all test cases under different mesh size and polynomial order. The further work will focus on comparing the order of accuracy of this DG frame under the same mesh level with the traditional FEA method. The code has the potential to be expanded to solve more complex thermal problems, such as detailed TEC modelling, full laser package thermal modelling etc. The further research will also be focused on combining the DG linear structure solver to simulate the TEC deformation under different thermal loads and flow conditions.

Reference

[1] Chen.W.H, Liao.C.Y, Hung.C.I, A numerical study on the performance of miniature thermoelectric cooler affected by Thomson effect, Applied Energy, **89**, 2012, pp.464-473.

[2] De Aloysio.G, De Monte.F, Thermal characterization of micro thermoelectric coolers: An analytical study, Journal of Physics: Conference Series Article 012007, **547**, 2014.

[3] Wang.C.C, Hung.C.I, Chen.W.H, Design of heat sink for improving the performance of thermoelectric generator using two-stage optimization, Energy, **39**, 2012, pp.236-245.

[4] Chen.M, Snyder.G.J, Analytical and numerical parameter extraction for compact modelling of thermoelectric coolers, International Journal of Heat and Mass Transfer, **60**, 2013, pp.689-699.

[5] Reed.W.H and Hill.T.R, Triangular mesh methods for the neutron transport equation, Los Alamos Scientific Laboratory Report, LA-UR-73-479, 1973.

[6] Chavent.G and Cockburn.B, The local projection p0-p1-discontinuous Galerkin finite element for scalar conservation laws, IMA Preprint Series #341, 1987.

[7] Bassi.F and Rebay.S, High-order accurate discontinuous finite element solution of the 2D Euler equations, Journal of Computational Physics, **138**, 1997, pp.251-285.

[8] Zengrong.H, Chunwe.G and Xiaodong.R, The Application of Discontinuous Galerkin Method in conjugate heat transfer simulations of gas turbines, Energies, **7**, 2014,pp.7857-7877.

[9] Huafei.S, Darmofal.L.D, An adaptive simplex cut-cell method for high-order discontinuous Galerkin discretizations of elliptic interface problems and conjugate heat transfer problems, Journal of Computational Physics, **278**, 2014, pp.445-468.

[10] Hesthaven.J.S and Warburton.T, Nodal Discontinuous Galerkin Methods, Algorithms, Analysis, and Applications, Springer, 2008.

[11] Chavent.G, A finite-element method for the 1-D water flooding problem with gravity, Journal of Computational Physics, **45**, 1982, pp307-344.

[12] William.D.H and Kyle.K.C, A composite grid solver for conjugate heat transfer in fluid-structure systems. Journal of Computational Physics,**228**, 2009,pp.3708-3741.

[13] Davis.G.D., Natural convection of air in a square cavity a bench mark numerical simulation, International Journal of Numerical Methods in Fluids,**3**,1983,pp.249-264.

[14] Basak.T, Anandalakshmi.R and Singh.A.K, Heatline analysis on thermal management with natural convection in a square cavity, Chemical Engineering Science, **93**, 2013, pp.67-90.